AI-Based Drag Reduction of a High-Speed Train Using Distributed Jets

G. H. Chang, B. F. Zhang, J. L. Liu, L. Shen, S. L. Tang, and Y. Zhou

Abstract This work studies experimentally the aerodynamic drag reduction (DR) of a high-speed maglev train (HSMT) model based on artificial intelligence (AI) control, following our successful campaign on the DR of Ahmed bodies. A highly streamlined 3-car HSMT model is used, and the Reynolds number *Re* is 4.0×10^5 based on the square root of the model cross-section. The aerodynamic drag of the model is measured using two force balances. More than 90 steady jets are deployed on the tail car, in which the dependence of DR on their blowing angles and blowing ratios is documented for each jet. The individual jets produce a maximum DR of 7% and a maximum net power saving of 4%. Seven spatially distributed jets are selected and an AI control system (Zhang et al. in Artificial intelligence control of a low-drag Ahmed body using distributed jet arrays. J Fluid Mech 963 [6]) is deployed to find the best strategies to combine the seven jets in terms of their blowing ratios. Both DR and control power input are incorporated in the cost function. The AI control discovers forcing that creates a DR of 10%. Furthermore, the net power saving reaches about 5% given a DR of 6%.

Keywords Artificial intelligence · Active control · High-speed maglev train · Drag reduction

G. H. Chang and B. F. Zhang are equally contributed.

G. H. Chang · B. F. Zhang · L. Shen · S. L. Tang · Y. Zhou (✉)
Centre for Turbulence Control, Harbin Institute of Technology, Shenzhen 518055, China
e-mail: yuzhou@hit.edu.cn

J. L. Liu
National Engineering Research Center for High-Speed EMU, CRRC Qingdao Sifang Co. Ltd., Qingdao 26611, China

D. Kim et al. (eds.), *Fluid-Structure-Sound Interactions and Control*, Lecture Notes in Mechanical Engineering, https://doi.org/10.1007/978-981-97-6211-8_10

1 Introduction

The State Council of China has announced its ambitious plan to raise the speed of high-speed trains (HSTs) to 400 km/h and even 600 km/h. One of the obstacles for such HSTs to be commercially viable is the rapidly rising aerodynamic drag with train speed. There have been a great number of attempts, as reported in the literature, on the aerodynamic drag reduction of HSTs using various passive techniques, e.g., aerodynamic shape optimizations [1, 2], vortex generator [3] and non-smooth surface [4]. These investigations have achieved a great success. However, when shaping vehicle bodies has reached or approached its optimum, it is active control that can potentially reduce aerodynamic drag significantly further. This has been demonstrated by our recent campaign on the active DR of Ahmed bodies [5, 6], in which the optimal combinations of actuations achieved maximum DRs of 32% and 21% for the high and low-drag regimes, respectively, based on the artificial intelligence (AI) control. Active DR, especially AI-based, for a high-speed train has been rarely studied. Note that both Ahmed bodies and HST tail car are critical geometries, i.e. the bluff body geometries that exhibit sharp flow transition when changing one of the geometrical parameters [7, 8]. One may naturally surmise that the knowledge we have gained from the study of Ahmed bodies might be to a certain extent applicable for HSTs. This work aims to address this issue and to develop an AI-based active DR technique, following our strategies deployed for the DR of Ahmed bodies, for a high-speed maglev train using combined steady jets.

2 Experimental Details

Experiments are conducted in a closed-circuit wind tunnel with a test section of 1.0 m high, 0.8 m wide and 5.6 m long. Experimental setup is schematically shown in Fig. 1. A 1/20 scaled highly streamlined three-car maglev HST model is examined, which has an overall length of 1.8 m, a width of 0.184 m and a height of 0.21 m. The Reynolds number Re investigated is 4.0×10^5 based on the square root of the model cross-section area. The model is supported by two cylindrical posts mounted on the head and tail trains. The other end of each supporting post is connected to a force balance, which is fixed on an aluminum plate mounted on a fixed frame outside and isolated from the wind tunnel. The total aerodynamic drag of the model is captured from the two force balances. Sixty pressure taps, connected to two pressure scanners, are distributed on the tail car to measure the surface pressure distribution.

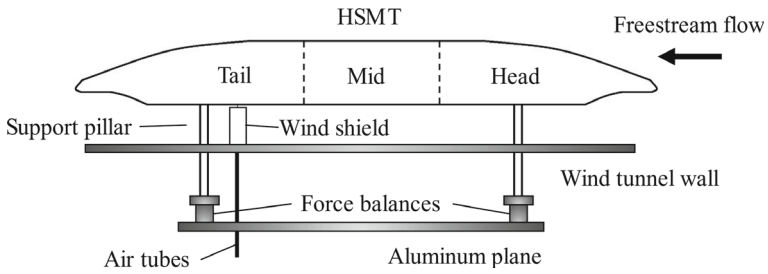

Fig. 1 Schematics of experimental setup

3 Results and Discussion

Over 90 different steady blowing actuations are investigated in Open-loop control experiment. Nevertheless, only twelve of them can achieve drag reduction. These actuations, referred to as S_i ($i = 1, 2, \ldots, 12$), are distributed in four specific areas (Fig. 2a), denoted as A_i ($i = 1, 2, \ldots, 4$). The actuation outlet is 1 mm in width and 23–42 mm in length. The blowing angles θ_{si} of S_i are defined with respect to the streamwise direction. The net power saving S is calculated by $(\Delta F U_\infty - 0.5\rho Q_{Si} V_{Si}^2 - p_{si} A_{si} V_{si})/F_D\, U_\infty$, where ΔF is the reduced drag under control, Q_{Si} is the flow rate of S_i, V_{Si} is the jet exit velocity, p_{si} is the mean static pressure of S_i, A_{si} is the outlet area of S_i, and F_D is the drag of the baseline flow. Positive value of DR or S represents drag reduced or power saved. Open-loop control results indicate that individual actuation S_1, distributed in area A_3 with $\theta_{s1} = 105°$, can produce a maximum DR of 7% but S is only −5%. Under this control, the surface pressure has been greatly increased as shown in Fig. 3a. The variation of surface pressure $\Delta C_p = C_{p,ctr} - C_{p,un}$, where $C_{p,ctr}$ represents surface pressure under control and $C_{p,un}$ represents surface pressure in baseline flow. As the pressure taps get closer to the tail nose, ΔC_p increase gradually. C_{p1}, the pressure taps in the symmetry plane and is closest to the tail nose, increases about 80%. ΔC_{p10} and ΔC_{p17} are 16% and 13%, respectively. It indicates that the jet from actuation S_1 weaken the longitudinal vortices above those two surfaces. While, the surface pressure recovers only in the area not far from the jet. Pressure taps away from S_1 remain consistent between baseline flow and controlled flow. When blowing angle of S_1 is adjusted to $\theta_{s1} = 90°$, S can achieve 4% when DR = 6%.

The AI control system, consisting of the sensing (force balances), actuations (blowing jets) and control (linear-genetic-programming-algorithm-based controller) units as well as the plant, is used to find the optimal blowing ratios of seven actuations with a view to maximizing the DR and S. Unsupervised learning of the optimal control is converged after 10 generations. Each generation consists of 100 samples. Each sample is tested for 40 s to estimate the cost J ($J = -\Delta F - C^*S + 0.4$), which $C = 0.1$ is the weighted constant aiming to teach control units the importance of power saving. A lower J denotes a better control effect. The learning curve is shown in Fig. 4, in which the square symbol represents the minimum cost J_n (the subscript

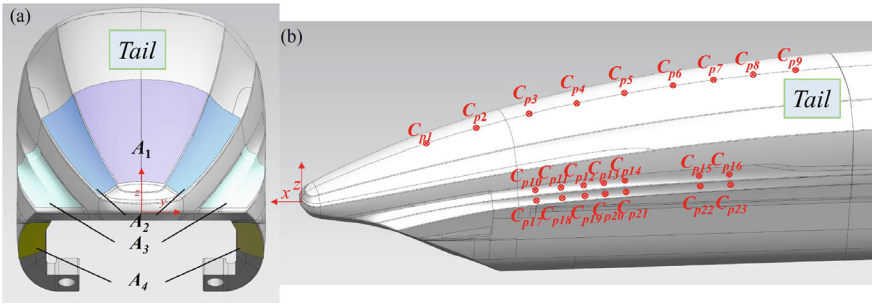

Fig. 2 **a** The areas A1 – A4 for the arrangement of actuations. **b** Measurement locations C_{p1} – C_{p23} of surface pressure

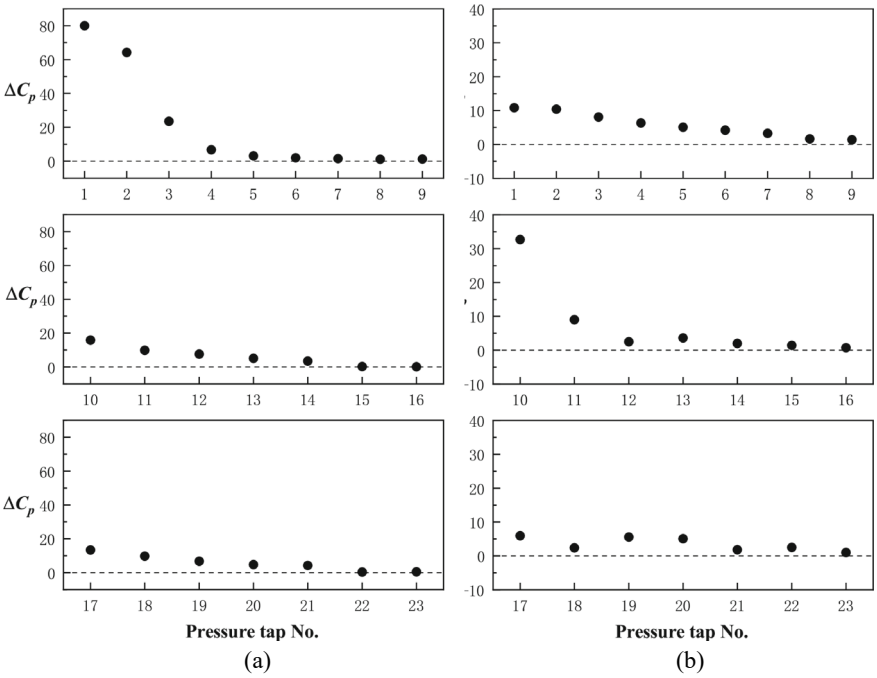

Fig. 3 Variation in $C_{p1} - C_{p23}$ under the optimal control of **a** S_1; **b** the most efficient control

'n' denotes the generation number) in each generation. Although the 100 samples of first generation are generated randomly, the AI system achieves the minimum cost $J_1 = 0.32$ corresponding to a DR of 8%, which is slightly larger than the maximum DR produced by the individual S_1 in the open-loop control experiment. As it evolves to the fourth generation, the cost declines to $J_4 = 0.31$ and achieves a DR = 8%. The cost of fifth generation keeps decreasing to $J_5 = 0.3$ and achieves a DR = 9%.

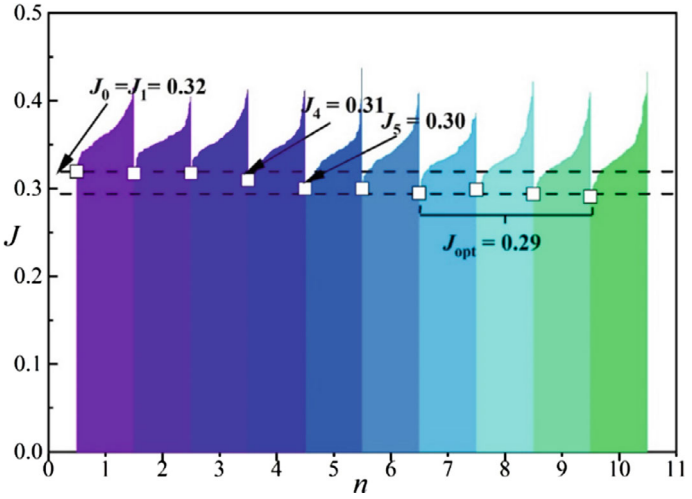

Fig. 4 Learning curve of AI control based on TGP

The costs of 7–10th generation remain unchanged and converge to an optimal cost $J_{\text{opt}} = 0.29$. The optimal combination can produce a DR of 10%.

Nevertheless, there is nearly no net power saving under the optimal combination. Based on analysis of the data generated from the learning process, a most efficient combination is found to yield a maximum S of 5%, with a DR of 6%. This sacrifice in DR which results in an increasement in S is achieved by cutting down the blowing ratios of actuations. Specifically, the input power of the most efficient combination is only 20% of that of the optimal combination. The surface pressure variation under this most efficient combination is shown in Fig. 3b. The largest ΔC_p appears at side surface, which may be connected to the weakening of the pair of longitudinal vortices formed at the lateral sides of the tail. Under optimal power saving combination, the pressure surface is recovered not only near the actuation, but also at far upstream area. Thus, the combination achieves a considerable DR with a very low input energy.

4 Conclusions

An extensive investigation on the active DR of a HSMT model using distributed jets has been conducted. In the open-loop control experiment, over 90 actuations, deployed at different locations of the tail car, had been investigated, in which the dependence of DR on their θsi and blowing ratio has been examined. The individual jet may achieve a maximum DR of 7% and a maximum net energy saving S of 4%. The surface pressure recovers greatly in the symmetry plane and slightly in the side surfaces. The pressure taps in the symmetry plane and nearest to tail nose can achieve a ΔCp of 80%. With seven jets blowing simultaneously, an AI control system

is deployed to find the best strategies in terms of their blowing ratios to maximize the DR of the model with the net power saving considered. An optimal strategy has been found to achieve DR = 10% after 10 generations of the learning process, though without net power saving. It is found that a small sacrifice in DR may achieve a much larger S. The most efficient control achieves $S = 5\%$ with a DR of 6%. The surface pressure recovers most in the side surface under this control. Work is under way to unveil the altered wake structures or the DR mechanisms under the optimal and the most efficient controls.

Acknowledgements YZ wishes to acknowledge support given to him from CRRC Qingdao Sifang Co. Ltd. through contract SF/GY-梁字-2021-244, NSFC through grant 91952204 and the Research Grants Council of the Shenzhen Government through grant JCYJ20210324132816040. BFZ is grateful for the support from NSFC through grant 12272114.

References

1. Muoz-Paniagua J, García J (2020) Aerodynamic drag optimization of a high-speed train. J Wind Eng Ind Aerodyn 204:104215
2. Wang S, Wang R, Xia Y, Sun Z, You L, Zhang J (2021) Multi-objective aerodynamic optimization of high-speed train heads based on the PDE parametric modeling (Article). Struct Multidiscip Optim 64(3):1285–1304
3. Krajnovic S (2009) Shape optimization of high-speed trains for improved aerodynamic performance. Proc Inst Mech Eng Part F J Rail Rapid Transit 223(F5):439–452
4. Wang DW, Chen CJ, Deng C (2020) The use of non-smooth surfaces to control the wake of a high speed train. Proc Inst Mech Eng Part F-J Rail Rapid Transit 234(9):1041–1053
5. Zhang BF, Liu K, Zhou Y, To S, Tu JY (2018) Active drag reduction of a high-drag Ahmed body based on steady blowing. J Fluid Mech 856:351–396
6. Zhang BF, Fan D, Zhou Y (2023) Artificial intelligence control of a low-drag Ahmed body using distributed jet arrays. J Fluid Mech 963
7. Morel T (1987) Aerodynamic drag mechanisms of bluff bodies and road vehicles. Springer, Boston, MA
8. Zhou Y, Zhang BF (2021) Recent advances in wake dynamics and active drag reduction of simple automotive bodies (Review). Appl Mech Rev 73(6)